Particle-in-liquid compound drops impact on solid wall: Spreading and retraction

Rui Wang and Chun-Yu Zhang [*]

Department of Modern Mechanics, University of Science and Technology of China, Hefei 230027, China

(Received 7 March 2024; accepted 18 November 2024; published 3 December 2024)

Impact of particle-in-liquid compound drops on solid wall is investigated numerically using a diffuse-interface immersed-boundary method. We focus on the effect of the properties of the particles on the spreading and retraction dynamics of the compound drops. Numerical simulation results reveal that with an increase in the particle volume fraction (α), there is a corresponding decrease in the volume of fluid involved in spreading. As a result, the presence of particles within the drops inhibits the spreading of the compound drops. Specifically, the maximal spreading ratio ($\beta_{\max}$) can be scaled by $1-\alpha$, analogous to the scaling observed in pure drops. Conversely, both the rebound coefficient and particle density exert minimal effect on $\beta_{\max}$ at same α. Additionally, the presence of particles is found to promote compound drop rebound, leading to a reduction in droplet-wall contact time.

DOI: 10.1103/PhysRevFluids.9.123601

I. INTRODUCTION

Impact of drops on solid walls is a common occurrence in both natural and industrial settings, including pathogen transport by raindrops [1], inkjet printing [2,3], spray cooling [4,5], and criminal forensics [6]. In many applications, drops are composed of multiple components, and their structures exhibit a variety of geometric shapes [7–10]. Among these structures, the core-shell structure of compound drops is the most widely used, in which one component is completely encapsulated in another [11]. In particular, compound drops consisting of solid particles encapsulated by a liquid shell have recently been proposed in several promising technologies, such as the rapid and controllable encapsulation of colloidal objects [12], the active emulsion made of drops encapsulating assemblies of active particles [13], and surface tension-driven colloidal motors [14]. Investigation of the dynamics of particle-in-liquid compound drops can offer theoretical insights into the preparation of specialized drops and the management of their behavior, potentially paving the way for a broad spectrum of applications in additive manufacturing and thermal spraying [15].

The spreading and retracting dynamics of a drop impacting on a substrate is governed by the interplay between inertia, surface tension, and viscosity. The interplay of these forces can be characterized by two dimensionless parameters, namely Reynolds number Re $(=\rho UD/\mu)$ and Weber number We $(=\rho U^2D/\sigma)$, where D, ρ, μ, σ and U are the diameter, density, viscosity, surface tension coefficient and impacting velocity of drop, respectively. The deformation of the drops during spreading and retracting can be quantified by the dimensionless spreading ratio, β, which represents the ratio of the diameter of the deformed droplet to its initial diameter. At the early stage of drop impact, a thin liquid film was formed in the contact area between the drop and the substrate. The radius of the wetted area was observed to evolve in a square-root law over time [16–18]. This behavior can be explained by establishing self-similar pressure and velocity fields near the contact

[*]Contact author: cyzhangcfd@ustc.edu.cn

area of the drop [19,20]. The thickness of the liquid film follows a 3/2 scaling law with respect to time [21]. At the maximum spreading of the drops, the maximal spreading ratio ($\beta = \beta_{\max}$) of liquid drops had been extensively studied and received significant attention [22–24]. Chandra and Avedisian [25] proposed a scaling law of $\beta_{\max} \sim Re^{1/5}$ by assuming that the kinetic energy is entirely consumed by viscous dissipation in the high viscosity limit. This scaling law has been shown to accurately predict experimental and numerical results [26,27]. Clanet *et al.* [26] reported a scaling law of $\beta_{\max} \sim We^{1/4}$ based on the balance between drop acceleration and Laplace pressure gradient at the side of the spreading drop in the limit of low viscosity. The scaling law $\beta_{\max} \sim We^{1/2}$ had also been proposed to describe drops impacting free-slip surfaces [28–30] and the maximum spreading of liquid-metal drops [31]. Additionally, the wettability of the substrate plays a crucial role in determining $\beta_{\max}$ [32–36]. Several universal models have been proposed to predict the maximum spreading of drops on no-slip substrates over a wide range of Re and/or We [29,37–39]. Notably, Wang *et al.* [39] developed a universal model that considers the effect of substrate wettability on $\beta_{\max}$ using a second-order Padé approximation,

$$\beta_{\max} Re^{1/5} = \frac{f(P)}{A_1 + f(P)}, \tag{1}$$

where $P = WeRe^{-4/5}(1-\cos\theta)^{-2}$, $f(P) = P^{1/4} + A_2 P^{1/2}$, $A_1 = 2$, and $A_2 = 10$ in a wide range of flow parameters: $10 < Re < 10000$, $20 < We < 1000$, and $30^\circ < \theta < 150^\circ$, where θ is the contact angle of the drop on the substrate. The universal model exhibits good agreement with prior experimental and numerical data [29,40–42]. At the stage of retraction [43], it was observed that the rate of drop retraction remained constant and was not affected by the impact velocity [27]. Drops may eventually rebound from the substrate [44–47]. The duration between the moment the droplet contacts the substrate and the moment it departs was known as the rebound time [48], which characterizes the temporal features of the droplet bouncing [47,49]. The rebound time was found to follow the scale of $\sim(D/U)We^{1/2}(1-\cos\theta)^{-1/2}$ when $\theta > 90^\circ$ [50]. More studies can be found in review articles [51–54].

In contrast to the impact of pure drops, the impact of compound drops is significantly influenced by the core structures. The core structures typically comprise liquid droplets [55–62], gas bubbles [63–68], solid particles [69,70], biological cells [71], and other components. In the investigations of liquid-in-liquid compound drops, Liu *et al.* [55] numerically simulated the volume fraction of core drop (defined by α) and the interface tension ratio effecting on the maximal spreading ratio ($\beta_{\max}$) of the compound drop with equal density between the core and shell drop. A modified Weber number was defined to quantify and successfully predicted $\beta_{\max}$ by substituting it into the model of Lee *et al.* [42], within the parameter range of $10 \leqslant We \leqslant 800$ and $Re = 1000$. Later, the effect of density contrast on $\beta_{\max}$ had also been numerically simulated and a new model had been proposed for a quantitative description [72]. Liu and Tran [60] experimentally investigated the impact of a compound drop consisting of oil (shell) and water (core). Two ejection lamellas were observed consisting of oil and water, and noted that the transition from spreading to splashing occurred by varying the volumetric oil ratio. Furthermore, the maximal spreading ratio of the compound drop depends on the impact velocity, the volumetric oil ratio, and the viscosity of the core drop, by mixing glycerol in water [61]. In addition, Blanken *et al.* [73] observed that the oil shell prevents contact between the water core and the solid surface due to the lubrication of the oil. For the air-in-liquid drops, Gulyaev and Solonenko [64] experimentally observed the formation of a counter jet in the impact of hollow glycerin drops. The volume of the counter jet was found to depend on the volume of the bubble, and was independent of the viscosity of the liquid and impact velocity [67]. To predict the maximal spreading ratio of the hollow drops, Naidu and Dash [67] proposed a model based on the energy interaction between the spreading liquid and the liquid in the counter jet. Numerical simulations by Wei and Thoraval [65] showed that the maximal spreading ratio of the hollow drops decreased with the addition of a bubble, due to a decrease in the initial kinetic energy with an increase in the volume ratio of the bubble. Comparatively, there are relatively

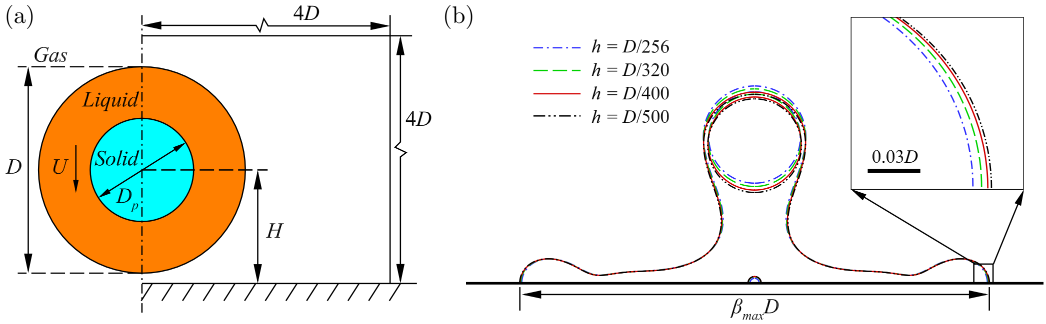

FIG. 1. (a) A sketch of a particle-in-liquid compound drop impacting onto a horizontal substrate at a vertical velocity U. The diameters of the whole compound drop and particle are D and D_p, respectively. (b) Convergence study with respect to the compound drop shape at the maximum spreading with $Re = 1000$, $We = 50$, and $\alpha = 0.125$. Different curves denote the numerical results with different mesh resolutions: $\Delta x = D/256$ (dash dotted), $D/320$ (dashed), $D/400$ (solid), and $D/500$ (dash dot dotted), respectively. The inset shows a zoomed-in view of the interface.

few studies on the impact of particle-in-liquid compound drops, as particles tend to attach more easily to the droplet interface [74,75]. However, the effect of the particle on the particle-in-liquid compound drops impacting onto solid substrate is lacking. Specifically, the volume, density, and coefficient of restitution of the particle on the spreading and retracting require investigation.

In this study, we numerically investigate the impact of particle-in-liquid compound drops. We examine the effect of varying volume ratio of particle to compound drop (denoted by α) on the spreading and retracting behavior, in the parameter space of $0 \leqslant \alpha \leqslant 0.422$, $20 \leqslant We \leqslant 1000$, and $20 \leqslant Re \leqslant 10\,000$. We then modify the $\beta_{\max}$ through α to obtain a universal model for the maximal spreading ratio of the compound drops. Additionally, the effects of coefficient of restitution and density of particle on $\beta_{\max}$ are also investigated. Furthermore, the rebound time of the compound drops is simulated. Our study found that the presence of particles not only inhibits the spreading of the compound drops but also reduces their rebound time.

II. PROBLEM STATEMENT AND NUMERICAL METHOD

A. Problem statement

We numerically investigate particle-in-liquid compound drops impacting onto a planar substrate. The simulation setup, as shown in Fig. 1(a), is axisymmetric and includes a compound drop surrounded by still gas. The density and viscosity ratios of the gas to the liquid are set to 0.0015 and 0.018, respectively, which are referenced to the ratio between air (density 1.2kg/m^3, viscosity 1.8×10^{-5}Pas) and 1 cSt silicone oil (density 0.81×10^3kg/m^3, viscosity 1.0×10^{-3}Pas) at room temperature 20 °C. The compound drop with a diameter D internally contains a concentric solid particle with a diameter of D_p. The volume fraction of the particle is defined as $\alpha = (D_p/D)^3$. The density ratio between particle and liquid is denoted by $\lambda_\rho = \rho_p/\rho$, where ρ_p is the density of the particle. Initially, the distance between the mass center of the particle and the wall is $H = 0.55D$. The computational domain is $4D \times 4D$. The boundary conditions are the symmetry condition at the left boundary, far-field condition at the right boundary, and no-slip condition at the upper and bottom boundaries. In the present study, the compound drops are of millimeter size with impact velocity on the order of 1 m/s. Accordingly, the gravity effect is negligibly small compared with the acceleration encountered in the drop impact ($\sim U^2/D$).

B. Numerical method

An axisymmetric diffuse-interface immersed-boundary (DIIB) method [76] is used to simulate the impact of particle-in-liquid compound drops on the walls. The DIIB method is a powerful tool for simulating incompressible multiphase flows that involve rigid objects of irregular shape and moving contact lines on a Cartesian mesh [77]. The liquid-gas interface is represented by the volume fraction of liquid, denoted as C_L, and its evolution is governed by the Cahn-Hilliard equation:

$$\frac{\partial C_L}{\partial t} + \nabla \cdot (\mathbf{u} C_L) = \frac{1}{Pe} \nabla^2 \psi, \tag{2}$$

where the chemical potential ψ is defined as

$$\psi = C_L^3 - 1.5C_L^2 + 0.5C_L - C_L C_S (1 - C_L - C_S) - Cn^2 \nabla^2 \psi, \tag{3}$$

the Cahn number $Cn\,(= 0.75\Delta x/D)$ is a measure of the thickness of a diffuse interface and Pélect number is set to $Pe = 0.9/Cn$ [78], where Δx is the mesh size of the Cartesian mesh. The distribution of the volume fraction of the solid, C_S, is prescribed according to the position of the sphere. To simulate the moving contact lines (MCLs) on the substrate and particle, we employed a characteristic MCL model [76,77], which updates C_L in the MCL region, according to the local normal direction and wettability of the substrate. The wettability of the substrate and particle are mainly prescribed by the contact angles θ and θ_p.

The governing equations for the flow velocity $\mathbf{u}$ and the pressure p are the dimensionless Navier-Stokes equations and continuity equation,

$$\rho\left(\frac{\partial \mathbf{u}}{\partial t} + \mathbf{u} \cdot \nabla \mathbf{u}\right) = -\nabla p + \frac{1}{Re} \nabla[\mu(\nabla \mathbf{u} + \nabla \mathbf{u}^T)] + \frac{\mathbf{f}_s}{We} + \mathbf{f}_{IB}, \tag{4}$$

$$\nabla \cdot \mathbf{u} = 0, \tag{5}$$

where the $\mathbf{f}_s$ is the surface tension and $\mathbf{f}_{IB}$ represents the additional force due to the presence of particles. When the particle is about to contact the substrate, a collision force model [76] is used to avoid the overlapping between the particle and the substrate. The repellent force f_c follows

$$f_c = \begin{cases} 0 & H - D_p/2 \geqslant 2\Delta x, \\ C_{\text{eff}}\left(\frac{H - D_p/2}{2\Delta x} - 1\right)^2 & H - D_p/2 < 2\Delta x \quad \text{and} \quad U_p < 0, \\ \varepsilon^2 C_{\text{eff}}\left(\frac{H - D_p/2}{2\Delta x} - 1\right)^2 & H - D_p/2 < 2\Delta x \quad \text{and} \quad U_p > 0, \end{cases} \tag{6}$$

where U_p is the velocity of the particle, and $U_p < 0$ indicates particle impact onto the substrate, while $U_p > 0$ signifies particle rebound from the substrate. In this study, the empirical coefficient is selected as $C_{\text{eff}} = 100 \times 0.5MU^2/(2\Delta x)$, where M is the mass of particle and $0.5MU^2$ denotes the initial kinetic energy of the particle. The value of C_{eff} is chosen to ensure that the particle's velocity is reduced to zero prior to contacting the wall. Assuming that a particle decelerates from an initial velocity U_i and rebounds with a velocity U_j, we have

$$\frac{1}{2} M U_i^2 = \int_{2\Delta x}^{H^*} C_{\text{eff}} \left(\frac{H - D_p/2}{2\Delta x} - 1\right)^2 dh,$$

$$\frac{1}{2} M U_j^2 = \int_{2\Delta x}^{H^*} \varepsilon^2 C_{\text{eff}} \left(\frac{H - D_p/2}{2\Delta x} - 1\right)^2 dh, \tag{7}$$

where H^* represents the distance between the particle and the wall when the particle's velocity decelerates to zero. Mathematically, $U_j = \varepsilon U_i$ can be derived. The coefficient of restitution, ε, is defined as the ratio of the particle's velocity after impact to that before impact on the substrate. For instance, $\varepsilon = 1$ corresponds to a completely elastic collision and $\varepsilon < 1$ corresponds to an incompletely elastic collision. More details of numerical implementation can be found in Liu *et al.* [76] and Liu and Ding [77].

The method has been successfully validated and applied for simulating the dynamics of a sphere impacting a liquid pool, as demonstrated in previous works [76,79–81]. To ensure the accuracy and reliability of the numerical results, the convergence of the simulation is examined by investigating the maximal spreading of the particle-in-liquid compound drop under the conditions of $Re = 1000$, $We = 50$, $\alpha = 0.125$, $\varepsilon = 1$, and $\lambda_\rho = 1$. Figure 1(b) presents snapshots of the compound drop at the maximal spreading, with mesh sizes of $\Delta x = D/256$, $D/320$, $D/400$, and $D/500$, respectively. The results indicate that the numerical solutions converge with mesh refinement, as evidenced by the consistent drop shape. Specifically, the numerical results obtained with $\Delta x = D/400$ are nearly indistinguishable from those obtained with the finest mesh size of $\Delta x = D/500$. Therefore, a Cartesian mesh with a mesh size of $\Delta x = D/400$ is employed in subsequent simulations. Additionally, a small bubble is entrapped under the center of the compound drop in Fig. 1(b), which is similar to the phenomenon observed in pure droplet impact experiments [82,83].

III. RESULTS AND DISCUSSION

Unless otherwise stated, the wettability of the substrate and particle, density ratio, and coefficient of restitution of the particle are fixed: $\theta = 90^\circ$, $\theta_p = 90^\circ$, $\lambda_\rho = 1$, and $\varepsilon = 1$. The dimensionless impact time t is rescaled by D/U, where $t = 0$ corresponds to the instant of contact between the drop and the substrate. In the present study, the compound drop is equivalent to a pure drop when $\alpha = 0$.

A. Flow features

Figure 2 illustrates the snapshots of particle-in-liquid compound drop impacting onto solid wall at $Re = 1000$, $We = 50$, and various volume fractions ($\alpha = 0.064$, 0.125, and 0.216, respectively). The results of pure drop ($\alpha = 0$) are included for a comparison of the impacting dynamics. At the early stage ($t \leqslant 0.25$), before the particles reach the substrate, they move synchronously with the drops and have a negligible effect on the surface of the compound drops. The surface shapes of the compound drops are almost identical to those of the pure drops. At the intermediate stage ($0.25 \leqslant t \leqslant 0.75$), the particles bounce off the substrate and move upwards. The particles carry some of the fluid with them resulting in less fluid in the part that is involved in spreading. As a result, the deformation of compound drops is reduced compared to pure drops [see the second panel of Figs. 2(a)–2(d)]. The deformation of the drops can be quantitatively described by the spreading ratio β. Note that the spreading ratio corresponds to the diameter of the contact line at the contact angle of 90°. At the moment when the compound drops reach their maximal spreading ($t = t_{\max}$), the presence of particles within the compound drops leads to a reduction in $\beta_{\max}$, regardless of whether the particles are moving downwards [e.g., $t = 1.76$ in Fig. 2(b)] or upwards [e.g., $t = 1.59$ in Fig. 2(c)] at this moment. Furthermore, $\beta_{\max}$ decreases with an increase in α. At the stage of drop retraction ($t > t_{\max}$), the liquid film at the contact line bulges. The presence of particles within the compound drops causes some of the fluid to accumulate at the center of the droplet. Eventually, interfacial rupture occurs in the compound drop [see $t = 3.16$ in Fig. 2(b)]. For sufficiently large particles, there will still be a continuous upward movement, even carrying some of the fluid away from the drop [74]. In summary, the presence of particles within the drops inhibits the spreading of the compound drops and facilitates the retraction process.

Figure 3 shows the time evolution of the spreading ratio (β) and the particle position (H) [see the definition in Fig. 1(a)] at $Re = 1000$ with various α and We. β is accurately measured based on the position of the contact line. Numerical results indicate that β initially increases to its maximum value ($\beta = \beta_{\max}$) over time during the spreading stage, and then decreases during the retraction stage. During the retraction stage, the evolution of the spreading ratio β over time becomes inconsistent, as evidenced by the intersecting curves, indicating that the particles introduce a nonlinear disturbance to the retraction process of the compound drops. The particles rebound upon impacting the substrate. For relatively large particles ($\alpha \geqslant 0.125$) and higher velocities ($We \geqslant 50$),

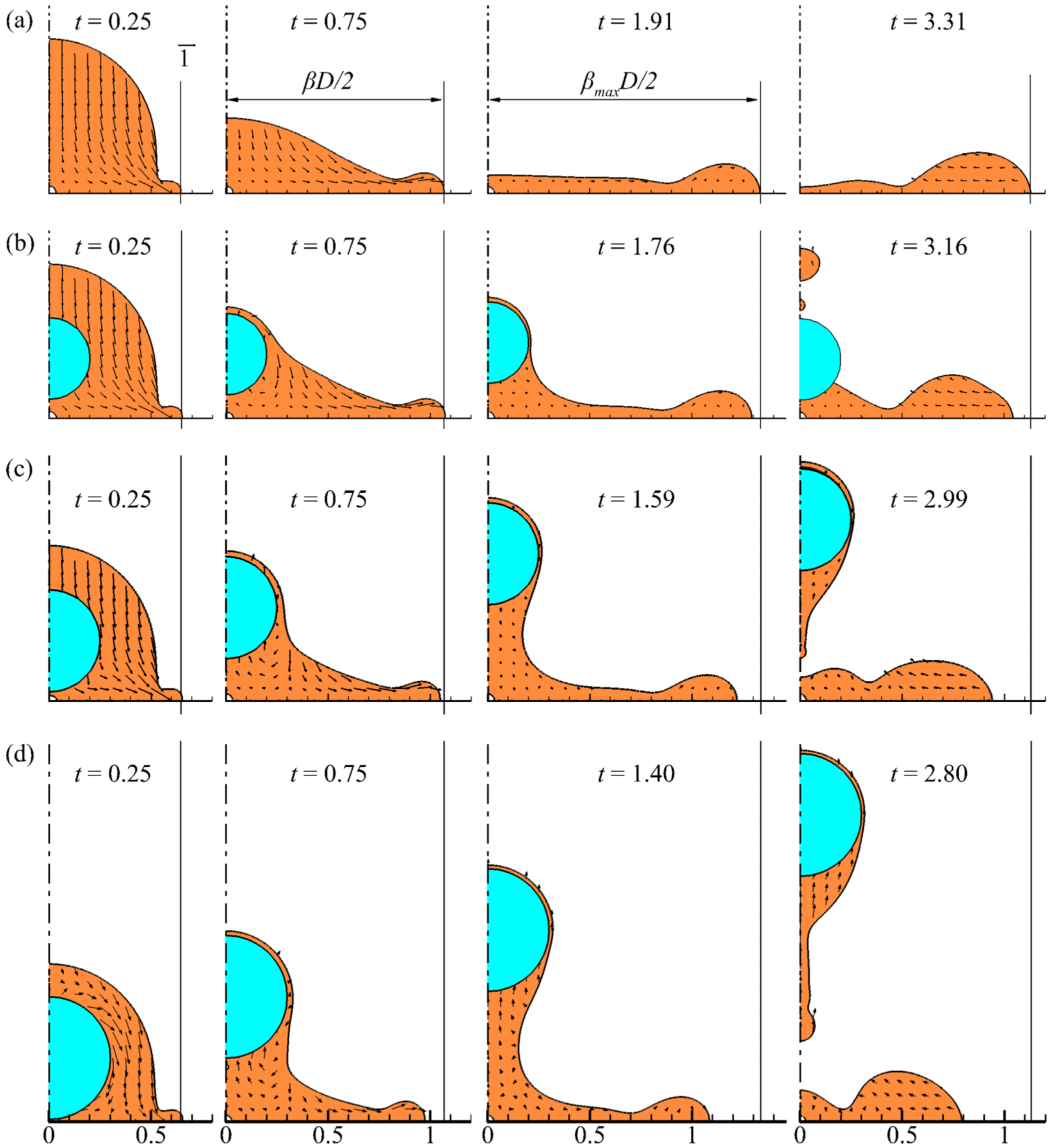

FIG. 2. Illustration of particle-in-liquid compound drop impacting onto solid wall at $Re = 1000$, $We = 50$, and various volume fractions: $\alpha = 0$ (a), 0.064 (b), 0.125 (c), and 0.216 (d). The columns from left to right correspond to different times: $t = 0.25$, 0.75, $t_{\max}$, and $t_{\max} + 1.4$, respectively. Here, $t_{\max}$ denotes the moment of the maximum spreading of the compound drop. Arrows in the fluid indicate the appropriate amount of velocity at the local point and arrows in the particles indicate the direction of motion and velocity of the particles. The reference velocity vectors are provided in (a) and the same one is used in each column. The movies of the impact dynamics can be seen in the Supplemental Material [84].

they will continue to ascend due to inertial effects, assuming negligible gravity. Conversely, smaller particles [e.g., $\alpha = 0.064$ in Fig. 3(a)] and lower velocities [e.g., $We = 20$ in Fig. 3(b)] exhibit weaker inertia, causing them to rise a limited distance before falling back and rebounding multiple times on the wall. Upon further analyzing the results, we find that with an increase of α at a fixed We, the maximal spreading ratio $\beta_{\max}$ and the moment of the maximal spreading $t_{\max}$ both decrease.

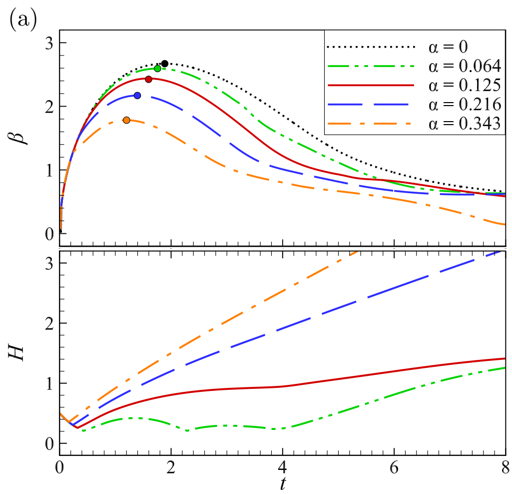

FIG. 3. Time evolution of the spreading ratio β and the particle position H at $Re = 1000$ with (a) a fixed We (=50) and various α, and (b) a fixed α (=0.125) and various We. The bullets on curves indicate the moment $\beta = \beta_{\max}$.

Conversely, $\beta_{\max}$ and $t_{\max}$ both increase with an increase of We at the same α. It is indicated that the presence of particles prevents the spreading of the compound drops. In most instances, the velocities of smaller particles and those with lower initial velocities decrease markedly after particles rebound. This decrease is attributed to the interaction between particle movement and drop deformation. Consequently, particle properties, such as volume fraction and impact velocity, play an important role in the spreading and retraction of the compound drops.

B. Effect of particle volume on maximum spreading of compound drop

The presence of solid particles inhibits the maximum spreading of the compound drops due to the reduction in the volume of fluid involved in spreading. The definition of the volume of fluid involved in spreading, V_s, is shown in Fig. 4(a). At the moment of the maximum spreading of the compound drops, the fluid involved in the spreading can be seen as a "pancake" shape with a

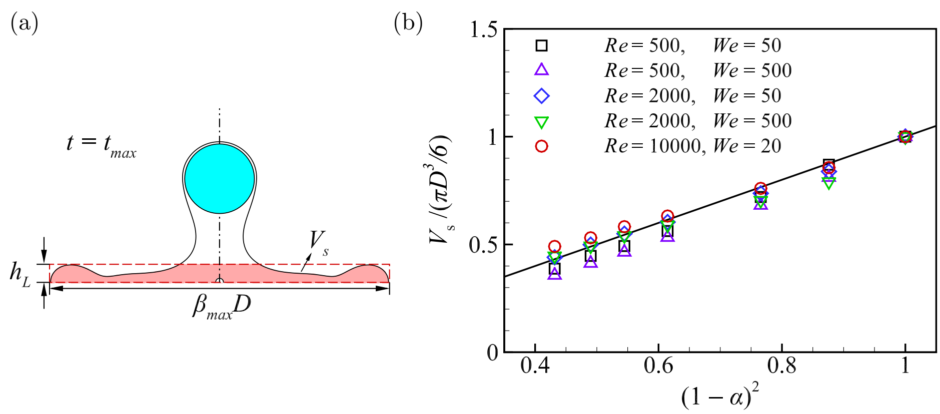

FIG. 4. (a) A sketch of the volume of fluid involved in spreading V_s. (b) $V_s/(\pi D^3/6)$ as a function of $1 - \alpha$ at various Re and We. The solid line represents the relation of $V_s/(\pi D^3/6) = (1 - \alpha)^2$.

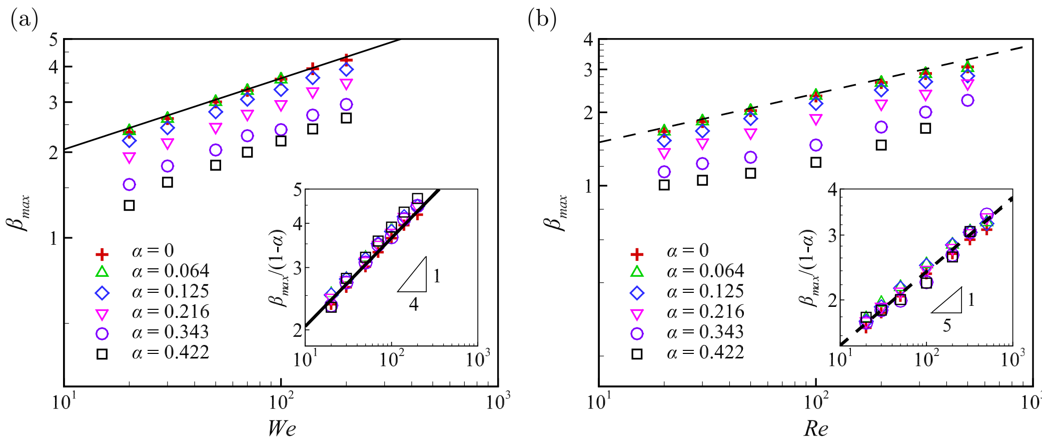

FIG. 5. Maximal spreading ratio as a function of (a) We at $Re = 10\,000$, and (b) Re at $We = 1000$. In (a), the solid line denotes $\beta_{\max} \sim We^{1/4}$. The inset shows the scaling law of $\beta/(1-\alpha) \sim We^{1/4}$. In (b), the dashed line denotes $\beta_{\max} \sim Re^{1/5}$. The inset shows the scaling law of $\beta/(1-\alpha) \sim Re^{1/5}$.

diameter $\beta_{\max} D$ and thickness h_L. Thus, the thickness h_L scales with $\sim V_s/(\beta_{\max}^2 D^2)$. For the case of maximum spreading of a pure drop, $V_s \sim D^3$ leads to $h_L/D \sim \beta_{\max}^{-2}$. However, the volume of fluid involved in the spreading of a compound drop is smaller. On the one hand, the initial fluid volume within the compound drop is relatively small, specifically $V_0 = (1-\alpha)\pi D^3/6$. On the other hand, a liquid film encapsulates the surface of the solid particles, and fluid is carried by these particles upon rebounding, further diminishing V_s. We assume that the volume of fluid carried by the particles is proportional to the particle volume, expressed as $k\alpha V_0$, where k is a fitting factor. Then, the volume of fluid involved in spreading is obtained by $V_s = (1-k\alpha)(1-\alpha)\pi D^3/6$. As shown in Fig. 4(b), numerical results for V_s agree well with the prediction with a fitting of $k = 1$. The numerical results indicate that V_s roughly follows a relation of $V_s/(\pi D^3/6) \approx (1-\alpha)^2$. Although the error grows as α increases, it remains within $\pm 10\%$. Therefore, we can express h_L as

$$\frac{h_L}{D} \sim \frac{(1-\alpha)^2}{\beta_{\max}^2}. \tag{8}$$

The maximal spreading ratio $\beta_{\max}$ of a particle-in-liquid compound drop is primarily influenced by We, Re, and α, as shown in Fig. 5. The numerical findings indicate that the maximal spreading ratio follows the scaling law of $\beta_{\max} \sim We^{1/4}$ at high Re ($= 10\,000$) and $\beta_{\max} \sim Re^{1/5}$ at high We ($= 1000$), which is consistent with the experimental and numerical results of pure drops [26,39]. For various values of α, $\beta_{\max}$ generally decreases with an increase of α at the same We or Re. Additionally, as illustrated in the insets of Fig. 5, the numerical results can be rescaled by $\beta_{\max}/(1-\alpha)$ and collapsed together,

$$\frac{\beta_{\max}}{1-\alpha} \sim We^{1/4} \quad \text{and} \quad \frac{\beta_{\max}}{1-\alpha} \sim Re^{1/5}. \tag{9}$$

To explain the scaling laws between $\beta_{\max}$, α, We, and Re, we follow the analysis of Clanet *et al.* [26]. First, the acceleration of the compound drops impacting on the substrate follows $a \sim U^2/D$. Thus, the thickness of the spreading liquid film can be measured in terms of the effective capillary length $h_L \sim \sqrt{\sigma/\rho a}$ in the limit of low viscosity ($Re = 1000$). By considering Eq. (8) for $0 \leqslant \alpha \leqslant 0.422$, we obtain $\beta_{\max}/(1-\alpha) \sim We^{1/4}$, which is in agreement with the numerical results shown in the inset of Fig. 5(a). Second, we assume that the kinetic energy of the fluid involved in spreading is proportional to $\rho_L V_s U^2$. We further assume that the upward movement of the particles consumes an additional portion of the kinetic energy used for spreading, which is proportional to

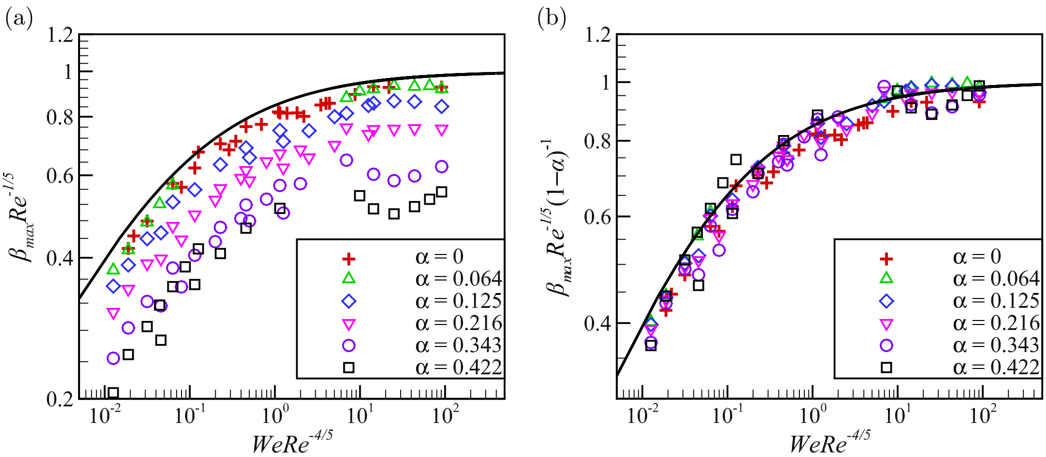

FIG. 6. (a) $\beta_{\max}Re^{-1/5}$ as a function of $WeRe^{-4/5}$. The dashed line denotes the prediction of (3.1). (b) The rescaled maximal spreading ratio $\beta_{\max}Re^{-1/5}/(1-\alpha)$ as a function of $WeRe^{-4/5}$. The solid lines denote the prediction of Eq. (10).

the volume fraction of the particles, i.e., $\alpha\rho_L V_s U^2$. The remaining kinetic energy used for spreading is then $\sim(1-\alpha)\rho_L V_s U^2$. For relatively large values of We ($=1000$), the kinetic energy is fully converted into viscous dissipation in the limit of $Re \leqslant 1000$, which is proportional to $\mu U\beta_{\max}^3 D^3/h_L$. This leads to the scaling law $\beta_{\max}/(1-\alpha) \sim Re^{1/5}$, which is consistent with the numerical results shown in the inset of Fig. 5(b). In summary, the scaling law for the rescaled maximal spreading ratio of particle-in-liquid compound drops, $\beta_{\max}/(1-\alpha)$, is similar to that of pure drops. Therefore, we can use the Padé approximation to describe the maximum spreading of compound drops and pure drops in a uniform scaling law,

$$\frac{\beta_{\max}Re^{1/5}}{1-\alpha} = \frac{f(P)}{A_1 + f(P)}, \tag{10}$$

where $P = WeRe^{-4/5}$, $f(P) = P^{1/4} + A_2P^{1/2}$, $A_1 = 2$, and $A_2 = 10$ for all cases. Figure 6(a) shows the $\beta_{\max}Re^{-1/5}$ versus $WeRe^{-4/5}$ in the range of $20 \leqslant Re \leqslant 10\,000$ and $20 \leqslant We \leqslant 1000$. All results in Fig. 6(b) collapse to the prediction of Eq. (10). It is noteworthy that the results for pure liquid drop ($\alpha = 0$) are also included here.

C. Effect of coefficient of restitution and particle density ratio on $\beta_{\max}$

The effect of the coefficient of restitution ε and the particle density ratio λ_ρ on the maximal spreading of compound drops is investigated. Figure 7 shows $\beta_{\max}$ as a function of We, Re, and α for various coefficients of restitution ε ranging from 0.25 to 1. Several observations are noteworthy. First, $\beta_{\max}$ follows the scaling laws of $\beta_{\max} \sim We^{1/4}$ at $Re = 10\,000$ (where inertia and surface tension dominate the compound drops), and $\beta_{\max} \sim Re^{1/5}$ at $We = 1000$ (where viscosity and inertia dominate the compound drops), both for a fixed $\alpha = 0.216$ and various ε. Second, $\beta_{\max}$ generally decreases with an increase of ε at constant We or Re. This decrease occurs because a higher particle rebound velocity allows particles to carry more fluid upwards, reducing the fluid involved in spreading, and consequently lowering $\beta_{\max}$. Notably, despite ε varying from 0.25 to 1 for different We or Re, the relative changes in $\beta_{\max}$ are all less than 8%. This suggests that the coefficient of restitution does not significantly affect on the maximal spreading of compound drops for a medium particle volume ($\alpha = 0.216$). Third, $\beta_{\max}$ is approximately proportional to $1-\alpha$ for various ε at $Re = 1000$ and $We = 50$, as shown in Fig. 7(c). For relatively small α, ε has minimal influence on $\beta_{\max}$. In contrast, for relatively large α, $\beta_{\max}$ increases as ε decreases. This is because, with a

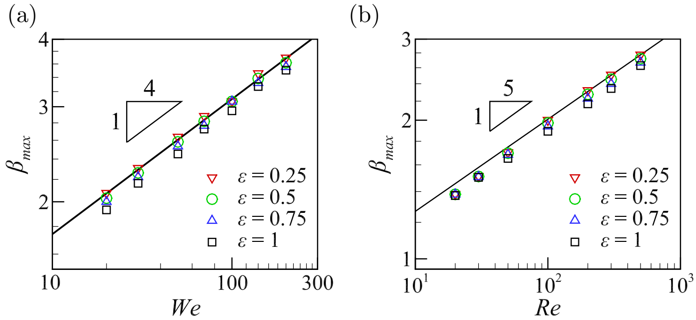

FIG. 7. With various coefficients of restitution ε, the maximal spreading ratio $\beta_{\max}$ as a function of (a) We at $Re = 10\,000$ and $\alpha = 0.216$, (b) Re at $We = 1000$ and $\alpha = 0.216$, and (c) α at $Re = 1000$ and $We = 50$.

smaller coefficient of restitution, particles rebound at a lower velocity and carry less fluid, thereby increasing the fluid volume involved in spreading. As a result, $\beta_{\max}$ increases by approximately 14% at $\varepsilon = 0.25$ compared to $\varepsilon = 1$ when $\alpha = 0.422$. Figure 8 shows the variation of $\beta_{\max}$ with We, Re, and α for different particle density ratios λ_ρ ($= 1 \sim 8$). At relatively high Re, the particle density has a negligible influence on β, as demonstrated by the results presented in Figs. 8(a) and 8(c), and for $Re \geqslant 300$ in Fig. 8(b). This phenomenon occurs because, in fluids with low viscosity, varying the particle density has minimal effect on the transported fluid volume, leaving the spreading fluid volume unaltered. Conversely, in high-viscosity fluids, heavier particles are less susceptible to deceleration, thereby exhibiting a greater capacity to transport fluid, potentially reducing β. Generally, the particle's coefficient of restitution and density ratio have a relatively minor effect on the maximum spreading compared to the particle volume ratio.

D. Effect of particle volume on rebound time

The rebound time of particle-in-liquid compound drops impacting hydrophobic surfaces is investigated at $\theta = 150^\circ$ and $Re = 1000$ with various α. We define the dimensionless time from the droplet's initial contact with the surface until it completely leaves the surface as the rebound time, denoted as t_R. Here, we chose the contact angle of $\theta = 150^\circ$ for drops to rebound easily. The drops typically rebound from the hydrophobic substrate, and the rebound time of pure drops follows the scaling law $t_R \sim We^{1/2}(1-\cos\theta)^{-1/2}$ [50,85]. Figure 9(a) shows the variation of the rebound time t_R of compound drops impacting hydrophobic surfaces. When particles impacting the surface rebound immediately, they not only inhibit drop spreading but also enhance drop rebound. The larger

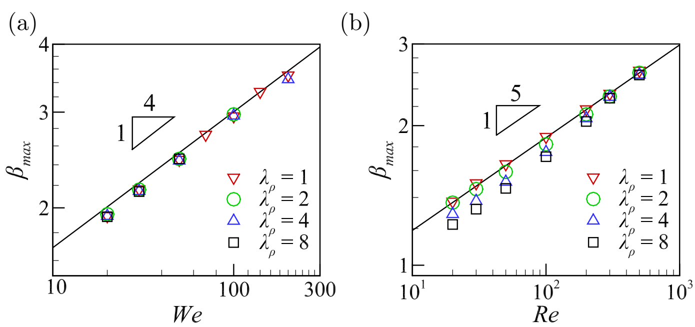

FIG. 8. The effect of various density of particle λ_ρ on $\beta_{\max}$ as a function of (a) We at $Re = 10\,000$ and $\alpha = 0.216$, (b) Re at $We = 1000$ and $\alpha = 0.216$, and (c) α at $Re = 1000$ and $We = 50$.

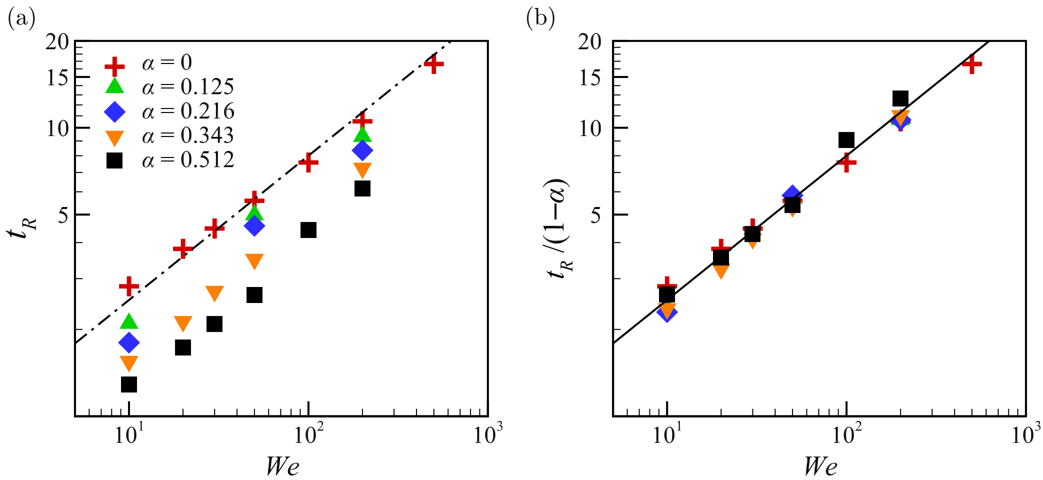

FIG. 9. (a) Rebound time t_R as a function of We at $Re = 1000$ with various α. (b) The scaling law of rescaled $t_R/(1-\alpha) \sim We^{1/2}$.

the particle volume, the more pronounced the effect of enhancing drop rebound. Hence, compared to the impact of pure drops, it can be expected that the rebound time of particle-in-liquid compound drops will be shorter. Similar to the analysis of compound drop spreading, we postulate that the rebound process also can be normalized by $t/(1-\alpha)$. Therefore, the rebound time of compound drops is expected to follow $t_R/(1-\alpha) \sim We^{1/2}$ at a fixed contact angle. Figure 9(b) shows the rescaled rebound time, revealing that the rebound times for various parameters approximately collapse onto the same curve, suggesting that our theoretical predictions for the contact time are consistent with the numerical results. Similarly, when $\alpha = 0$, our prediction for t_R also agrees with the theoretical formula of previous studies [85], further evidencing that our theory integrates the effects of pure drops and particle-in-liquid compound drops.

IV. CONCLUSION

We conduct a numerical investigation into the impact of particle-in-liquid compound drops on solid wall using the DIIB method, with the aim of gaining an understanding of the role of particle properties in the spreading and retraction of the compound drops. The presence of particles is found to inhibit the spreading of the compound drops. Specifically, with an increase in the particle volume fraction (α), there is a noticeable decrease in the spreading ratio (β). This behavior can be attributed to the fact that the larger particles make a reduction in the volume of the fluid involved in spreading (V_s). Numerical results suggest that V_s is proportional to $(1-\alpha)^2$. Similarly to the analysis of the pure drops spreading, the maximal spreading ratio $\beta_{\max}$ of the compound drops can be rescaled by $1-\alpha$ and collapsed to the scaling laws $\beta_{\max}/(1-\alpha) \sim We^{1/4}$ and $\beta_{\max}/(1-\alpha) \sim Re^{1/5}$. Furthermore, we introduce a Padé approximation with the same parameters in Wang *et al.* [39], which allowes us to collapse all results onto a unified prediction within the ranges of $20 \leqslant We \leqslant 1000$ and $20 \leqslant Re \leqslant 10\,000$. Additionally, we examine the effects of the rebound coefficient and the density of particles on $\beta_{\max}$ at the same α and find them to have minimal influence. We also investigate the rebound time of particle-in-liquid compound drops when impacting hydrophobic surfaces. Similarly to pure drops, the rebound time (t_R) can be rescaled by $1-\alpha$ and follows a comparable scaling law $t_R/(1-\alpha) \sim We^{1/2}$. However, it should be noted that research on the impact dynamics of particle-in-liquid compound drops remains limited. Scenarios such as drops containing multiple small particles or particles attached to the drop surface have not been extensively explored. Additionally, the wettability of the particles and the substrate may also play an important role in the spreading and rebound of the compound drops. Further research is needed to better understand the behavior of these drops and their interactions with particles and solid walls.

ACKNOWLEDGMENT

We are grateful for the support of the National Natural Science Foundation of China (Grants No. 12302342, No. 11932019, and No. 12388101).

The authors report no conflict of interest.

---

[1] S. Kim III, H. Park, H. A. Gruszewski, D. G. Schmale III, and S. Jung, Vortex-induced dispersal of a plant pathogen by raindrop impact, Proc. Natl. Acad. Sci. USA **116**, 4917 (2019).

[2] D. Lohse, Fundamental fluid dynamics challenges in inkjet printing, Annu. Rev. Fluid Mech. **54**, 349 (2022).

[3] B. Derby, Inkjet printing of functional and structural materials: Fluid property requirements, feature stability, and resolution, Annu. Rev. Mater. Res. **40**, 395 (2010).

[4] F. M. Tenzer, I. Roisman V, and C. Tropea, Fast transient spray cooling of a hot thick target, J. Fluid Mech. **881**, 84 (2019).

[5] J. Breitenbach, I. V. Roisman, and C. Tropea, From drop impact physics to spray cooling models: a critical review, Exp. Fluids **59**, 55 (2018).

[6] F. R. Smith, C. Nicloux, and D. Brutin, Influence of the impact energy on the pattern of blood drip stains, Phys. Rev. Fluids **3**, 013601 (2018).

[7] C.-Y. Zhang, J.-L. Chen, L.-J. Qian, and H. Ding, Two-dimensional Janus drops in shear: deformation, rotation and their coupling, J. Fluid Mech. **976**, A29 (2023).

[8] C.-Y. Zhang, P. Gao, E.-Q. Li, and H. Ding, On the compound sessile drops: configuration boundaries and transitions, J. Fluid Mech. **917**, A37 (2021).

[9] M. J. Neeson, R. F. Tabor, F. Grieser, R. R. Dagastine, and D. Y. C. Chan, Compound sessile drops, Soft Matter **8**, 11042 (2012).

[10] X. Hao, T. Du, H. He, F. Yang, Y. Wang, G. Liu, and Y. Wang, Microfluidic particle reactors: From interface characteristics to cells and drugs related biomedical applications, Adv. Mater. Interfaces **9**, 2102184 (2022).

[11] N. Blanken, M. S. Saleem, M.-J. Thoraval, and C. Antonini, Impact of compound drops: A perspective, Curr. Opin. Colloid Interface Sci. **51**, 101389 (2021).

[12] M. M. Norton, T. Brugarolas, J. Chou, D. Lee, and H. H. Bau, Ellipsoidal particles encapsulated in droplets, Soft Matter **10**, 4840 (2014).

[13] K. Xie, B. Gorin, R. T. Cerbus, L. Alvarez, J.-M. Rampnoux, and H. Kellay, Activity induced rigidity of liquid droplets, Phys. Rev. Lett. **129**, 138001 (2022).

[14] S. C. Ganesh, J. Koplik, J. F. F. Morris, and C. Maldarelli, Dynamics of a surface tension driven colloidal motor based on an active Janus particle encapsulated in a liquid drop, J. Fluid Mech. **958**, A12 (2023).

[15] W. Song, S. Yang, M. Fukumoto, Y. Lavallee, S. Lokachari, H. Guo, Y. You, and D. B. Dingwell, Impact interaction of in-flight high-energy molten volcanic ash droplets with jet engines, Acta Mater. **171**, 119 (2019).

[16] G. Riboux and J. M. Gordillo, Experiments of drops impacting a smooth solid surface: A model of the critical impact speed for drop splashing, Phys. Rev. Lett. **113**, 024507 (2014).

[17] S. Lejeune, T. Gilet, and L. Bourouiba, Edge effect: Liquid sheet and droplets formed by drop impact close to an edge, Phys. Rev. Fluids **3**, 083601 (2018).

[18] S. Lejeune and T. Gilet, Drop impact close to the edge of an inclined substrate: Liquid sheet formation and breakup, Phys. Rev. Fluids **4**, 053601 (2019).

[19] J. Philippi, P.-Y. Lagree, and A. Antkowiak, Drop impact on a solid surface: short-time self-similarity, J. Fluid Mech. **795**, 96 (2016).
[20] L. Gordillo, T.-P. Sun, and X. Cheng, Dynamics of drop impact on solid surfaces: evolution of impact force and self-similar spreading, J. Fluid Mech. **840**, 190 (2018).
[21] M. Usawa, Y. Fujita, Y. Tagawa, G. Riboux, and J. M. Gordillo, Large impact velocities suppress the splashing of micron-sized droplets, Phys. Rev. Fluids **6**, 023605 (2021).
[22] T. C. de Goede, K. G. de Bruin, N. Shahidzadeh, and D. Bonn, Predicting the maximum spreading of a liquid drop impacting on a solid surface: Effect of surface tension and entrapped air layer, Phys. Rev. Fluids **4**, 053602 (2019).
[23] M. J. Gordillo, G. Riboux, and E. S. Quintero, A theory on the spreading of impacting droplets, J. Fluid Mech. **866**, 298 (2019).
[24] Y.-F. Wang, Y.-B. Wang, X. He, B.-X. Zhang, Y.-R. Yang, X.-D. Wang, and D.-J. Lee, Scaling laws of the maximum spreading factor for impact of nanodroplets on solid surfaces, J. Fluid Mech. **937**, A12 (2022).
[25] S. Chandra and C. T. Avedisian, On the collision of a droplet with a solid surface, Proc. R. Soc. London A **432**, 13 (1991).
[26] C. Clanet, C. Beguin, D. Richard, and D. Quere, Maximal deformation of an impacting drop, J. Fluid Mech. **517**, 199 (1999).
[27] D. Bartolo, C. Josserand, and D. Bonn, Retraction dynamics of aqueous drops upon impact on non-wetting surfaces, J. Fluid Mech. **545**, 329 (2005).
[28] J. Eggers, M. A. Fontelos, C. Josserand, and S. Zaleski, Drop dynamics after impact on a solid wall: Theory and simulations, Phys. Fluids **22**, 062101 (2010).
[29] S. Wildeman, C. W. Visser, C. Sun, and D. Lohse, On the spreading of impacting drops, J. Fluid Mech. **805**, 636 (2016).
[30] J.-T. Zhang, H.-R. Liu, and H. Ding, Head-on collision of two immiscible droplets of different components, Phys. Fluids **32**, 082106 (2020).
[31] R. McGuan, R. N. Candler, and H. P. Kavehpour, Spreading and contact-line arrest dynamics of impacting oxidized liquid-metal droplets, Phys. Rev. Fluids **6**, L111601 (2021).
[32] M. Damak and K. Varanasi, Expansion and retraction dynamics in drop-on-drop impacts on nonwetting surfaces, Phys. Rev. Fluids **3**, 093602 (2018).
[33] A. Nasto, P.-T. Brun, and A. E. Hosoi, Drop impact on hairy surfaces, Phys. Rev. Fluids **4**, 064004 (2019).
[34] A. Russo, M. Icardi, M. Elsharkawy, D. Ceglia, P. Asinari, and C. M. Megaridis, Numerical simulation of droplet impact on wettability-patterned surfaces, Phys. Rev. Fluids **5**, 074002 (2020).
[35] J. C. Fernandez-Toledano, B. Braeckeveldt, M. Marengo, and J. De Coninck, How wettability controls nanoprinting, Phys. Rev. Lett. **124**, 224503 (2020).
[36] M. Wörner, Maximum spreading of an impacting drop, Int. J. Multiphase Flow **167**, 104528 (2023).
[37] N. Laan, K. G. de Bruin, D. Bartolo, C. Josserand, and D. Bonn, Maximum diameter of impacting liquid droplets, Phys. Rev. Appl. **2**, 044018 (2014).
[38] J. B. Lee, N. Laan, K. G. de Bruin, G. Skantzaris, N. Shahidzadeh, D. Derome, J. Carmeliet, and D. Bonn, Universal rescaling of drop impact on smooth and rough surfaces, J. Fluid Mech. **786**, R4 (2016).
[39] R. Wang, Y.-Z. Shi, C.-Y. Zhang, and H. Ding, On the maximal spreading of drops impacting onto a no-slip substrate, Phys. Fluids **34**, 052103 (2022).
[40] M. Pasandideh-Fard, Y. Qiao, S. Chandra, and J. Mostaghimi, Capillary effects during droplet impact on a solid surface, Phys. Fluids **8**, 650 (1996).
[41] D. C. Vadillo, A. Soucemarianadin, C. Delattre, and D. C. D. Roux, Dynamic contact angle effects onto the maximum drop impact spreading on solid surfaces, Phys. Fluids **21**, 122002 (2009).
[42] J. B. Lee, D. Derome, R. Guyer, and J. Carmeliet, Modeling the maximum spreading of liquid droplets impacting wetting and nonwetting surfaces, Langmuir **32**, 1299 (2016).
[43] F. Wang and T. Fang, Retraction dynamics of water droplets after impacting upon solid surfaces from hydrophilic to superhydrophobic, Phys. Rev. Fluids **5**, 033604 (2020).
[44] M. Y. Pack, A. Yang, A. Perazzo, B. Qin, and H. A. Stone, Role of extensional rheology on droplet bouncing, Phys. Rev. Fluids **4**, 123603 (2019).

[45] H. Zhan, C. Lu, C. Liu, Z. Wang, C. Lv, and Y. Liu, Horizontal motion of a superhydrophobic substrate affects the drop bouncing dynamics, Phys. Rev. Lett. **126**, 234503 (2021).
[46] P. K. Sharma and H. N. Dixit, Regimes of wettability-dependent and wettability-independent bouncing of a drop on a solid surface, J. Fluid Mech. **908**, A37 (2021).
[47] H. Zhao, X. Han, J. Li, W. Li, T. Huang, P. Yu, and L. Wang, Numerical investigation of a droplet impacting obliquely on a horizontal solid surface, Phys. Rev. Fluids **7**, 013601 (2022).
[48] J. C. Bird, R. Dhiman, H.-M. Kwon, and K. K. Varanasi, Impact of compound drops: A perspective, Nature (London) **503**, 385 (2013).
[49] X. Han, J. Li, X. Tang, W. Li, H. Zhao, L. Yang, and L. Wang, Droplet bouncing: Fundamentals, regulations, and applications, Small **18**, 2200277 (2022).
[50] S.-R. Gao, B.-J. Wei, J.-X. Jin, J.-S. Ye, Y.-F. Wang, S.-F. Zheng, Y.-R. Yang, and X.-D. Wang, Contact time of a droplet impacting hydrophobic surfaces, Phys. Fluids **34**, 067104 (2022).
[51] A. L. Yarin, Drop impact dynamics: Splashing, spreading, receding, bouncing.., Annu. Rev. Fluid Mech. **38**, 159 (2006).
[52] C. Josserand and S. T. Thoroddsen, Drop impact on a solid surface, Annu. Rev. Fluid Mech. **48**, 365 (2016).
[53] X. Cheng, T.-P. Sun, and L. Gordillo, Drop impact dynamics: Impact force and stress distributions, Annu. Rev. Fluid Mech. **54**, 57 (2022).
[54] H. Wang, H. Lu, and W. Zhao, A review of droplet bouncing behaviors on superhydrophobic surfaces: Theory, methods, and applications, Phys. Fluids **35**, 021301 (2023).
[55] H.-R. Liu, C.-Y. Zhang, P. Gao, X.-Y. Lu, and H. Ding, On the maximal spreading of impacting compound drops, J. Fluid Mech. **854**, R6 (2018).
[56] D. Baumgartner, G. Brenn, and C. Planchette, Effects of viscosity on liquid structures produced by in-air microfluidics, Phys. Rev. Fluids **5**, 103602 (2020).
[57] M. Piskunov, A. Semyonova, N. Khomutov, A. Ashikhmin, and V. Yanovsky, Effect of rheology and interfacial tension on spreading of emulsion drops impacting a solid surface, Phys. Fluids **33**, 083309 (2021).
[58] M. Piskunov, A. Ashikhmin, N. Khomutov, and A. Semyonova, Effects of wall temperature and temperature-dependent viscosity on maximum spreading of water-in-oil emulsion droplet, Int. J. Heat Mass Transf. **185**, 122442 (2022).
[59] S. Farokhirad, P. Solanky, and M. M. Shad, Spreading, breakup, and rebound behaviors of compound droplets impacting on microstructured substrates, Langmuir **39**, 3645 (2023).
[60] D. Liu and T. Tran, Emergence of two lamellas during impact of compound droplets, Appl. Phys. Lett. **112**, 203702 (2018).
[61] D. Liu and T. Tran, The ejecting lamella of impacting compound droplets, Appl. Phys. Lett. **115**, 073702 (2019).
[62] J. M. Zhang, E.-Q. Li, and S. T. Thoroddsen, Fine radial jetting during the impact of compound drops, J. Fluid Mech. **883**, A46 (2020).
[63] P. Gao and J. J. Feng, Spreading and breakup of a compound drop on a partially wetting substrate, J. Fluid Mech. **682**, 415 (2011).
[64] I. P. Gulyaev and O. P. Solonenko, Hollow droplets impacting onto a solid surface, Exp. Fluids **54**, 1432 (2013).
[65] Y. Wei and M.-J. Thoraval, Maximum spreading of an impacting air-in-liquid compound drop, Phys. Fluids **33**, 061703 (2021).
[66] Z. Fang, M. E. Taslim, and K.-T. Wan, Sloshing resonance of an acoustically levitated air-in-liquid compound drop, Langmuir **38**, 15534 (2022).
[67] D. P. Naidu and S. Dash, Impact dynamics of air-in-liquid compound droplets, Phys. Fluids **34**, 073604 (2022).
[68] V. A. Thale, M. Abouelsoud, H. Chizari, and M.-J. Thoraval, Impact force of an air-in-liquid compound drop, Phys. Fluids **36**, 022110 (2024).
[69] D. Zang, X. Wang, X. Geng, Y. Zhang, and Y. Chen, Impact dynamics of droplets with silica nanoparticles and polymer additives, Soft Matter **9**, 394 (2013).

[70] U. Banerjee, S. K. Jain, and A. K. Sen, Particle encapsulation in aqueous ferrofluid drops and sorting of particle-encapsulating drops from empty drops using a magnetic field, Soft Matter **17**, 6020 (2021).
[71] S. Tasoglu, G. Kaynak, A. J. Szeri, U. Demirci, and M. Muradoglu, Impact of a compound droplet on a flat surface: A model for single cell epitaxy, Phys. Fluids **22**, 082103 (2010).
[72] Z. Zhang, C.-Y. Zhang, H.-R. Liu, and H. Ding, Impact dynamics of compound drops of fluids with density contrast, J. Fluid Mech. **964**, A34 (2023).
[73] N. Blanken, M. S. Saleem, C. Antonini, and M.-J. Thoraval, Rebound of self-lubricating compound drops, Sci. Adv. **6**, eaay3499 (2020).
[74] W. Zhao, S. Lin, L. Chen, E. Q. Li, S. T. Thoroddsen, and M.-J. Thoraval, Jetting from an impacting drop containing a particle, Phys. Fluids **32**, 011704 (2020).
[75] F. Z. DeSoete, N. Passade-Boupat, L. Talini, F. Lequeux, and E. Verneuil, Stability of particle laden interfaces of drops flowing through a pore, Phys. Rev. Fluids **7**, 104002 (2022).
[76] H. R. Liu, P. Gao, and H. Ding, Fluid-structure interaction involving dynamic wetting: 2D modeling and simulations, J. Comput. Phys. **348**, 45 (2017).
[77] H. R. Liu and H. Ding, A diffuse-interface immersed-boundary method for two-dimensional simulation of flows with moving contact lines on curved substrates, J. Comput. Phys. **294**, 484 (2015).
[78] H. Ding, P. D. M. Spelt, and C. Shu, Diffuse interface model for incompressible two-phase flows with large density ratios, J. Comput. Phys. **226**, 2078 (2007).
[79] Y. Zhu, H.-R. Liu, K. Mu, P. Gao, H. Ding, and X.-Y. Lu, Dynamics of drop impact onto a solid sphere: Spreading and retraction, J. Fluid Mech. **824**, R3 (2017).
[80] H. Chen, H. R. Liu, X. Y. Lu, and H. Ding, Entrapping an impacting particle at a liquid–gas interface, J. Fluid Mech. **841**, 1073 (2018).
[81] H. Chen, H. R. Liu, P. Gao, and H. Ding, Submersion of impacting spheres at low Bond and Weber numbers owing to a confined pool, J. Fluid Mech. **884**, A13 (2020).
[82] S. Thoroddsen, T. Etoh, K. Takehara, N. Ootsuka, and A. Hatsuki, The air bubble entrapped under a drop impacting on a solid surface, J. Fluid Mech. **545**, 203 (2005).
[83] W. Bouwhuis, R. C. A. van der Veen, T. Tran, D. L. Keij, K. G. Winkels, I. R. Peters, D. van der Meer, C. Sun, J. H. Snoeijer, and D. Lohse, Maximal air bubble entrainment at liquid-drop impact, Phys. Rev. Lett. **109**, 264501 (2012).
[84] See Supplemental Material at http://link.aps.org/supplemental/10.1103/PhysRevFluids.9.123601 for four movies showing impact dynamics of drops at $Re = 1000$ and $We = 50$ with $\alpha = 0$, 0.064, 0.125 and 0.216, respectively.
[85] D. Richard, C. Clanet, and D. Quere, Contact time of a bouncing drop, Nature (London) **417**, 811 (2002).